Journal of Engineering Science and Technology
Vol. 18, No. 5 (2023) 2254 - 2268


# FRACTURE MECHANISM ANALYSIS OF BONE SCAFFOLD UNDER TENSILE LOAD: THE EFFECT OF POROSITY

AB AZIZ BIN MOHD YUSOF[1,*], MOHD AL FATIHHI MOHD SZALI JANUDDI[2], HASZEME ABU KASIM[1], AHMAD NAJMIE RUSLI[1], NOOR HAFIZ NOORDIN[1], MUHAMMAD NAZIF HAMZAH[2]

[1]School of Mechanical Engineering, College of Engineering, Universiti Teknologi MARA, UiTM, Johor Branch, Campus Pasir Gudang, 81750, Masai, Johor, Malaysia
[2]Advanced Facilities Engineering Technology Research Cluster (AFET), Plant Engineering Technology (PETech) Section, Malaysian Institute of Industrial Technology, Universiti Kuala Lumpur, Malaysia
*Corresponding Author: abaziz86@uitm.edu.my

## Abstract

Using bone scaffolds in tissue engineering is an important alternative to regenerate loose bone and promote cell adhesion. The main element of the bone scaffold is porosity. However, this porosity affects the structure's strength and leads to fracture when exposed to simulated mechanical load. Thus, this study aimed to investigate the effect of porosity on the strength of bone scaffold structures based on the fracture mechanism. The study used experimental and Finite Element Analysis (FEA) methods to analyse the effect of porosity between 0% to 70%. Three samples with 0%, 50%, and 60% porosity were then used to validate the FEA model. The study showed that the maximum tensile force decreases exponentially as porosity increases. The experiment revealed an 81% and 64% reduction in maximum tensile force for 0% and 30% porosity, respectively. The FEA results also demonstrated a similar pattern, with an 81% and 68% reduction in maximum tensile force for 0% and 30% porosity, respectively. The average difference between each porosity in the experiment was 38%, while the FEA results showed a 37% difference. The study found that the maximum tensile stress experienced by the bone scaffold decreases as the porosity increases, with a 55% average difference between the experimental and FEA results. The study's findings suggest that porosity significantly affects the strength of bone scaffold structures. Therefore, proper consideration is necessary while designing a bone scaffold to ensure it is mechanically suited and compatible with cell attachment for tissue engineering. Although the stress experienced by the structure was similar to that experienced by the material properties of PLA under strain, the study highlights the importance of understanding the effect of porosity on bone scaffold strength for efficient tissue engineering.

Keywords: Bone scaffold, Fracture mechanics, Porosity, Tension test.

## 1. Introduction

Replacing the missing bone with a bone scaffold is a promising alternative to traditional tissue engineering and regenerative treatments [1]. This method kick-starts the bone healing process by allowing osteoinducible cells to attach to the scaffold's surface and begin the bone remodelling process to replace the missing bone properly [1]. The bone scaffold offers many advantages, including speeding up the healing process, especially in cases where large voids form in the affected bone [2]. Additionally, bone scaffolds can act as biofactors that influence the seeded cells [3].

Designing a bone scaffold with suitable porosity and pore size is crucial, as this determines cell mobility, nutrient flow, and waste production [4, 5]. The pore architecture also affects the scaffold's mechanical properties, which are essential to withstand the working load and prevent fractures. Despite the advancements in the development of bone scaffolds for tissue engineering applications, the fracture behaviour of these structures has received relatively little attention in the literature [6]. Additionally, the effect of porosity on bone scaffold fracture behaviour has not been extensively studied.

Further improvement of bone scaffold design requires a better understanding of the scaffold's mechanical properties, including plasticity and crack propagation [7]. While current developments focus on the scaffold's functionality under recognised working loads, such as elastic modulus, yield strength, and tensile strength, little attention is given to the scaffold's fracture properties [8-10]. Fracture significantly affects the scaffold's functionality and can lead to significant problems, including reduced energy absorption [11]. Recent studies have explored the scaffold's durability in terms of strength and fracture properties, which is critical to establishing the structure's service life [11, 12]. Particularly in weight-bearing situations, bones are typically subjected to tensile forces that affect the durability of the bone scaffold for regenerative treatments.

The fracture behaviour of the bone scaffold can be described based on the experimental study and extended computational study [9, 11, 13, 14]. The disk-shaped compact tension fracture test is one of the tests to investigate the structure's fracture mechanics. The method was used to examine the failure of the porous structure under tensile loading by looking at its failure characteristics with proper consideration [15-17]. At the same time, further investigation could continue based on the computational study. Design parameters of the bone scaffold, such as porosity, young's modulus, and dissolution rate, could be optimised and obtained faster using Finite element analysis, FEA or Computational fluid dynamics CFD to suit the loading condition. The methods have proven their capability to investigate the behaviour and characteristics of the bone scaffold systematically.

A study on the bone scaffold was carried out by Huo et al. [18]. The study used Finite element analysis, FEA and uniaxial compression to explore the fracture caused by uneven stress-strain distribution on the structure. While studies done by Byrne et al. [8] reported the effect of porosity and its relation to bone formation. The study shows that the rate of bone formation increased with the porosity as it achieved 50 per cent tissue generation after three weeks. One of the latest study done by Carlsson et al. [11] on fracture behavior of human trabecular bone using both experiments and simulations. The experiments showed complex crack evolution with multiple crack fronts and arrests. The largest normal strains were

less than 4% in uncracked regions, indicating the applicability of the small deformation capability.

Manufacturing of bone scaffolds using additive manufacturing or 3D printing is driving tissue engineering further [19, 20]. The bone scaffold commonly produces from synthetic materials like Poly-lactic acid, PLA [10, 19, 21]. PLA can promote cell adhesion, proliferation, and differentiation, as it has been shown to support the growth of various types of cells, including bone cells. The material can be easily processed into various scaffold geometries using techniques such as 3D printing.

A study by Jia and Wang [22] and Wang et al. [23] proved the capability of the 3D printing method to mimic the microstructure inspired by nature and help to optimise the characteristics. Further, improve the bone scaffold done by Mohammadi et al. [19] using 3D printing of PLA-Gr-Mg composite. Mg improved the mechanical performance of the PLA-Gr-Mg composite under tensile and compression. The bonding quality between layers of the 3D-printed PLA-Gr sample was also enhanced, leading to better mechanical strength.

Properly designing and managing the bone scaffold's functionality to cope with interest is crucial in tissue engineering and regenerative treatment. Fracture is a failure mode that significantly affects functionality and leads to other significant problems. However, less attention was given to fracture of bone scaffold fracture. As this study aims to explore the effect of porosity on bone scaffold reflective cracking under tensile load, thus the study was focused on the bone scaffold's functionality under its recognised working loads. The study used 3D printing technology to fabricate bone scaffolds with different porosity levels and PLA material due to its compatibility with bone scaffold applications and availability for 3D printing [1, 5, 21, 24].

The study's novelty lies in focusing on the fracture behaviour of bone scaffolds and the importance of considering this aspect in designing and optimising the scaffold's functionality. In addition, the use of 3D printing technology to fabricate bone scaffolds and the effect of porosity on reflective cracking under tensile load were also explored.

## 2.Method

### 2.1. Sample model and fabrication process

Bone scaffold specimens with different percentages of porosity were modelled using Solidworks (Dassault Systèmes, USA) and then were fabricated using a 3D printer ( Ender-3 V2 3D Printer, Creality). The specimens were constructed by printing the filament and depositing the PLA material layer upon layer until the entire model was completed as 3D porous network to allow the fluid to flow in all directions [25]. To cope with speed and printing resolution (low layer height), only a 2mm printing layer height is used.

To capture design features, the print process was set to produce the specimens with a 0.1 mm profile and 0.2 mm nozzle size. Important to note that by increasing the specimen's porosity, the difficulty of the model increases as the structure becomes thinner and structure tolerance becomes hard to achieve. A quality check was carried out on every specimen before proceeding with the experiment to ensure the model was produced correctly.

The model for FEA and specimen for the experiment was built as in Fig. 1; with the detail tabulated in Table 1. In this study, six specimens were produced from the solid model with no porosity to the model specimen of 30%, 40%, 50%, 60%, and 70% porosity. The specimens' porosity varied by increasing the size of the circular hole applied to the bone scaffold. This design was proven its effectiveness based on the scaffold's mechanical properties and ability to support cell attachment and growth. This basic structure of a bone scaffold refers to its composition, porosity, and pore size [10, 26].These specimens were then used in FEA and the disk-shaped compact tension fracture test experiment.

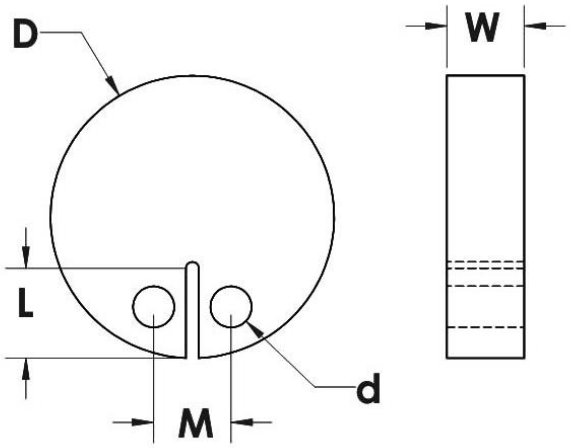


**Fig. 1. Model of disk-shape sample used in experimental and simulation study.**

**Table 1. Detailed dimensions of the sample model.**

| Notation | Detail | Dimension (mm) |
|---|---|---|
| D | Sample Diameter | 22.0 |
| W | Sample Width | 6.0 |
| L | Notch length | 7.0 |
| M | Distance | 6.0 |
| d | Loading hole | 3.2 |

The deformation on the specimen is based on the tension extended from elastic deformation to the plastic region. Therefore, the local stress distribution around the notch during the tensile can be obtained based on the FEA, representing the fracture behaviour of the 3D printing bone scaffold manufactured from PLA material.

## 2.2. Experimental testing

The experiment was conducted to collect the data according to the disk-shaped compact tension fracture test referring to ASTM standard E1820 [16, 17, 17, 27]. The specimen was attached to the customed jig, as shown in Fig. 2. The test specimens were allowed to rotate freely in the loading axis during the test.

A tensile test was performed by stressing the specimens with a constant displacement rate of 1.0 mm/min. Displacement and reaction force acting during

the test was recorded for data analysis and validation. At the same time, structure deformation was observed for the comparison with the FEA result in the next section. The first experiment used a solid specimen without porosity. The study was then repeated using five more specimens with a per cent porosity of 30% to 70%, as shown in Fig. 2.

A tensile test was performed by stressing the samples with a constant displacement rate of 1.0 mm/min. Based on ASTM standard E1820, mode one was preferred in the study, where the crack direction was expected to be perpendicular to the tensile load . Displacement and reaction force acting during the test was recorded for data analysis and validation. At the same time, structure deformation was observed to be compared against the FEA result in the next section.

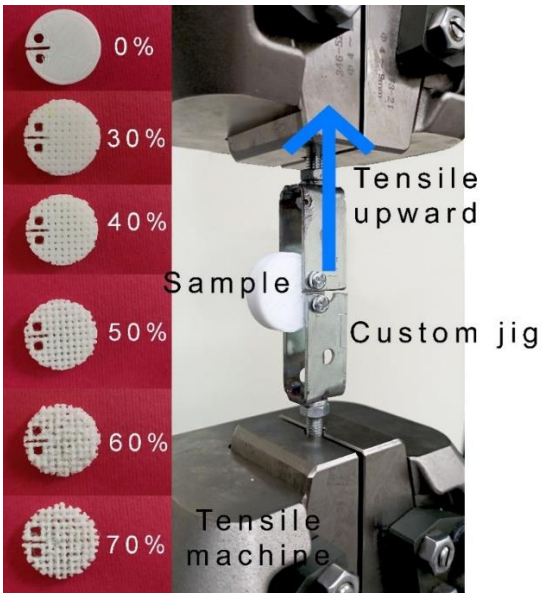


**Fig. 2. Experimental setup and samples.**

The first experiment was conducted using a solid sample without porosity. The study was then repeated using five more samples with a per cent porosity of 30% to 70%, as shown in Fig. 2.

## 2.3. Finite element simulation

Finite element analysis, FEA, was performed using the ABAQUS software package. The model was built using Solidworks software, as in Fig. 3. The material properties of PLA were considered in the experiment since PLA is the material for the bone scaffold and is easily available for fabrication using the 3D printing process. The material properties in stress-strain are detailed by Baheti et al. (2013) [29] reported the Neat PLA material. The data was obtained based on the uniaxial tensile test. The referred data was known as engineering stress and engineering strain. The material properties are divided into three regions, elastic, hardening and softening, which then need to process further before they can be imported into ABAQUS.

Figure 3 shows the model of FEA, and 1008MPa Young's modulus was extracted from the elastic region. A density of 1200kg/m$^3$ and a Poisson ratio of 0.36 was assigned to the model, respectively. The PLA materials were dealt with as Solid homogeneous, where the material properties are uniform across the sample and behave the same in all directions.

Meanwhile, the hardening and softening of the PLA after passing the elastic region are represented in Fig. 3. The plastic hardening was dealt with as isotropic. The conversion of the engineering stress-strain to true stress-strain was according to the formula True strain, $\varepsilon_{true} = log\ (1 + \varepsilon_{eng})$ and True stress, $\sigma_{true}=\varepsilon_{eng}*(1+\sigma_{eng})$.

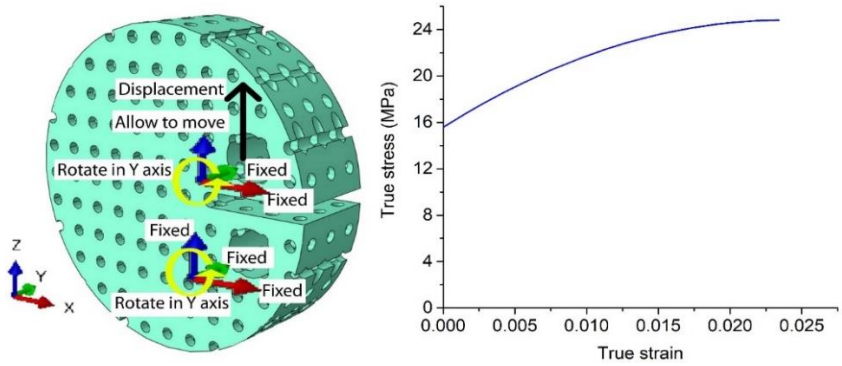


**Fig. 3. FEA model and applied boundary condition**.

Boundary conditions were set at loading holes, as shown in Fig. 1. The upper loading hole was established to allow it to move vertically on the Z-axis while rotating on the Y-axis with the displacement increment applied in the experiment (please refer to Section 2.3). Fixed boundary conditions were used at the X, Y and Z axes but allowed to rotate in the Y-axis to cope with the tensile load as it ramped up during the test.

Models of bone scaffolds meshed with tetra element C3D10M, a 10-node modified quadratic tetrahedron where the high plasticity deformation happens during the tensile test as it involves large deformation. Besides, consider the element error of highly stressed deformation. The models converged around 100k to 150k number of elements. The disk-shaped compact tension fracture test was analysed using a general static step where the displacement was applied slowly by ramping the same as the experiment. Besides, the effect of nonlinearities present in the material and geometry can be included in the analysis.

## 3. Result

### 3.1. Force/displacement validation

Validation of FEA based on the experiment was carried out using three samples of 0%, 50% and 60% porosity. The validated FEA setting was then used to study the effect of porosity on stress distribution on the bone scaffold structure. How porosity affects the strength of the structure that leads to the fracture was explored in detail. Figure 4 shows the graph of the tensile force versus displacement for both experiment and FEA. Based on the graph, FEA predicted the bone scaffold behaviour under

tensile load. As displacement ramped up, the PLA disk experienced tensile. The tensile force increased linearly in the elastic deformation region.

As the deformation kept increasing, passing the elastic limit, the shape alteration permanently increased the plasticity until it reached the ultimate stress. The ultimate stress can be noticed quickly and happens at 1.9 mm displacement for the 0% porosity sample. However, earlier ultimate stress was reached for the 50% and 60% porosity at 0.9 mm and 1.2 mm, respectively. Force reduction happens once the curve passes the ultimate stress in which the material softens toward the fracture point. Consideration of material fracture property was neglected. Thus, the simulation stopped between the ultimate stress and fracture point.

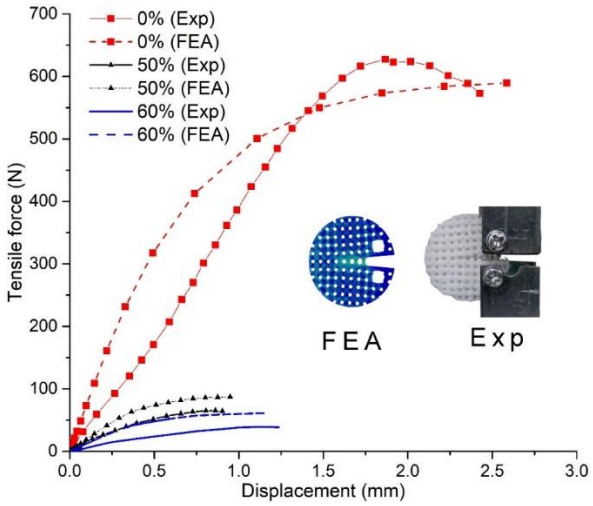


**Fig. 4. Load-crack opening displacement curve from experiment and FEA analysis and sample fracture during the test.**

Generally, the 0%, 50% and 60% graphs show a similar pattern: the tensile force increased with the displacement up to the maximum tensile force before reducing toward the softening region. The average percentage of error of FEA compared to experimental data for the three graphs was 21%. This evaluation is based on the maximum tensile force the bone scaffold can support. The disparity between FEA and experimental value happens because of several factors. The first factor was the difference in terms of the structural model between the FEA and the experimental samples.

In the FEA study, the model was perfectly homogenous. However, experiment samples were made layer by layer according to additive manufacturing, which reduced the sample's homogeneity from what was expected. Besides that, the resolution of the printing process reduces the tolerance of the geometry of the sample, especially on the critical structure, thus reducing its strength.

## 3.2. Peak load vs porosity

Figure 5 shows the maximum tensile stress experienced by the bone scaffold for both experiment and FEA. This maximum tensile test was extracted from the load-crack opening displacement curve, as shown in Fig. 4, and represented as a bar chart for

better comparison. Generally, the experimental and FEA results show the same reduction pattern as porosity increased and the maximum tensile force decreased exponentially, with the average error percentage for all data at a 55% difference.

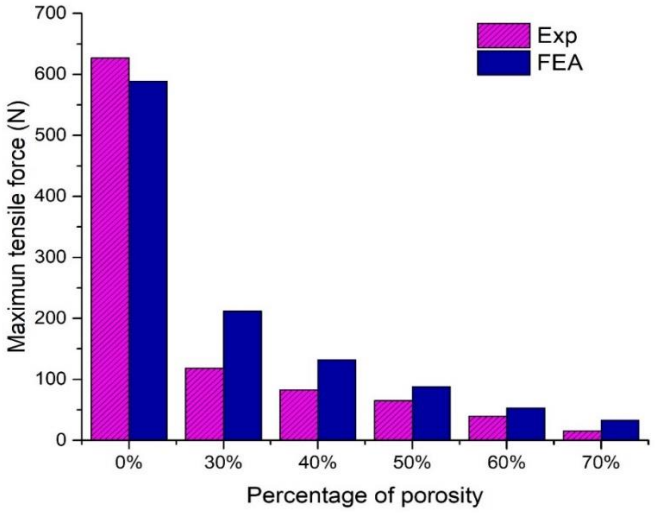


**Fig. 5. The maximum tensile force versus percentage of porosity for experimental test and FEA.**

However, in terms of per cent reduction, the experimental data show only a 1% difference as porosity increased. The average difference between each porosity in the experiment is 38%, compared to 37% obtained from FEA. This value was calculated by taking the total percentage difference between the lower and higher porosity's maximum tensile force. The maximum tensile force was reduced as the porosity increased from 0% to 30% at 81% and 64%, respectively, for the experiment and FEA.

Meanwhile, 30% to 40%, 30% and 38% force reduction happen. For 40% to 50%, 22% force reduction happened in the experiment, while 33% force reduction happened in FEA. Between 50% to 60%, the same reduction of 40% happens for both experiment and FEA. The last translation of 60% to 70%, 62% and 38% reduction happened for the experiment and FEA, respectively.

### 3.3. Structure deformation

Stress distribution focused on the notch tip of the sample during the tensile test. The concentrated region triggered cracking, which propagated across the sample. The stress distribution for the 0% sample was highly concentrated around the notch. The printing orientation, which happened at a 45-degree orientation, was much influenced by the crack propagation.

Meanwhile, the sample with higher porosity had horizontal crack propagation, as shown in Fig. 6. Overall maximum stress indicated by the 0% model was lower than the maximum stress experienced by the model with higher porosity, which was about 112% higher for the whole model structure.

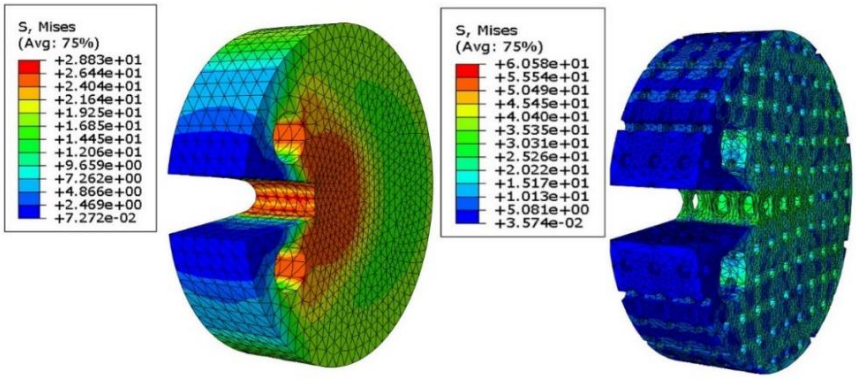


**Fig. 6. Stress distribution on the sample that concentrated on the notch during the test.**

## 3.4. Stress distribution near the tip of the crack

The stress experienced across the middle of the sample where the stress was concentrated at the same location for all samples modelled. Figure 7 shows the von Mises stress for all the samples based on the FEA. The graph was plotted as von Mises stress versus network pillar location. Distance between locations was 2 mm, representing the centre of circular shape for 30%, 40%, 50%, 60%, and 70% porosity. Even though 0% of pores experience higher maximum tensile force compared to the sample with higher porosity (refer to Fig. 5), a different result was obtained regarding the stress experienced at the crack region.

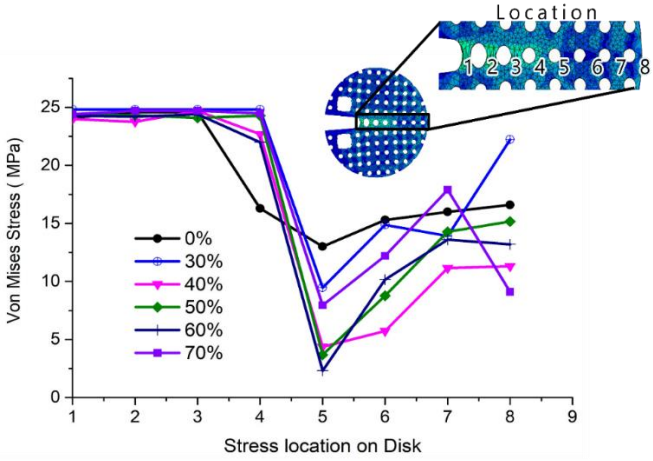


**Fig. 7. Stress distribution of 8 locations across the disk model for the different porosity for 3mm displacement.**

All samples show the same graph pattern and stress value of 24 MPa at the location close to the notch where the crack was triggered (range 0 to 6 mm). However, most experienced stress reduction to 7 MPa at the location 8mm from

the notch. After 8 mm or the fifth location, the stress value gradually increases, up to location 7 mm or 17 mm before the rate increment reduces toward location 8mm or 16mm away from the notch.

The aspect was related to the reduction of the pillar cross-section. This happened as the porosity increased with circular diameter. With 6 mm sample widths, the area of the wall pillar was 7.1 $mm^2$ for 30% of porosity, 6.1 $mm^2$ for 40% of porosity, 5.1 $mm^2$ for 50% of porosity, 4.2 $mm^2$ for 60% of porosity, and 3.3 $mm^2$ for 70% of porosity. The area was reduced linearly to about one $mm^2$. The percentage difference in areas between other porosities was 14%, 16%, 17% and 21% (for example, between 30 with 40 was 14%, and 40 with 50 was 16%, etc.)

## 4. Discussion

The experimental test and FEA result show a 21% error percentage disparity for comparing the force-displacement curve (Fig. 4). At the same time, a 1% difference for maximum tensile force versus the percentage of porosity is shown in Fig. 5. These two comparisons were carried out to ensure proper validation was considered for this study and to improve the reliability of the reported result. The disparity happens because of two factors: the construction of the model and material behaviour due to the printing process [23].

The first reason explains that the disk's porosity increased from 30% to 70%, causing the bone scaffold structure to be thinner and increasing the difficulty of the printing process, which reduced the specimen detail. In addition, the factor related to the bone scaffold structure's size and resolution reduction affects the geometry detail and refinement of the additive manufacturing. Moreover, a micro void exists between the printed layer due to printing limitations, reducing strength and stiffness [23, 30]. The second reason is that since the experimental specimen is produced by 3D printing, the specimen exhibits anisotropic behaviour due to the building orientation and printing strategy of deposited material layer-by-layer to create the product [17, 23]. However, the FEA simplified the model by assigning homogenous properties to PLA. This simplified the experimental study as the material properties are uniform without the irregularity of additive manufacturing [16].

Introducing pores to the bone scaffold structure modified the stress distribution compared to the solid disk specimen or zero per cent porosity. Under tensile load, stress is concentrated around the notch (refer to Fig. 6) for zero per cent porosity, which triggers a crack and then propagates depending on the printing orientation. On the other hand, stress distribution for the porous structure demonstrates different characteristics, which is higher on the middle vertical column. Higher stress on the middle column occurs as the vertical column support most of the applied load. As a result, the solid disk's stress is 52% lower than the porous structure (Refer to Fig. 6). Besides that, higher stress is also indicated in vertical columns compared to the horizontal column, as the vertical column supports most of the tensile load compared to the horizontal column.

Fracture and crack at the tip related to local stress plasticity that increased and caused instability, leading to fracture. The mode type of fracture observed in experimental testing is a thin crack crosswire along its centre as displaced fracture forms a gap where the disk break. The crack tends to propagate along the contour straight without changing its direction. The cracking location is the lowest hardness of the material since stress is concentrated, causing higher plasticity deformation.

A higher force impacts the bone scaffold more than it can support. Mechanically under loading conditions, the bone scaffold undergoes elastic deformation where the stress is directly proportional to the applied strain. Plastic deformation then happens when it exceeds the yield stress.

The fracture has happened as the ability to the plastic deformation is exhausted. The main factor in the fracture is the crack propagation movement and the resistance to crack movement by the stronger structure. Resistance to crack encourages increasing plastic flow stress which causes bone scaffold to deform constantly. The samples' fracture was related to the concentrated stress on the structure. It happens as a crack propagates across the diameter while the tensile increase above the yield stress reaching the strain-softening, causing the deterioration of material strength

Changing the porosity for the same material properties, PLA consequently alters the stiffness and strength of each model [31]. As shown in Fig. 5, maximum tensile stress reduces exponentially from an average of 600 N to 24 N, respectively, for 0% to 70% of porosity. The shape change causes this 96% reduction in maximum stress from solid to porous. The fracture characteristics of the specimen are directly linked to the size of the middle column structure that bridges the top and bottom disk during the test.

The fracture happens by concentrating the stress and then debonding the top and bottom at the notch location. As the first column elongates with the higher strain, the deformation is then transferred to the second column and subsequently. The elastic deformation can be seen from the elongation of the vertical column after 0.6mm. The column was elongated as the displacement increased from 0.6 mm to 1 mm vertically. At this moment, the bone scaffold started showing strain hardening as it reached maximum tensile force. After passing maximum tensile force, the material lost its strength and began to soften until it almost reached fracture.

In this study porosity of the disk was manipulated, causing a reduction in the column's structure thickness which alters the disk's volume. Figure 7 shows the stress value across the pore disk, meaning the stress's magnitude is the same for all specimens, while the force-load reduction is captured as in Fig. 4 and across the different structure porosity. The stress-strain curve behaviour can be used to explain the result. As the displacement increased during the tensile test, the internal stress gradually built up according to equation $\sigma = E\varepsilon$ where $\sigma$, $E$, and $\varepsilon$ respectively, for stress experienced by the PLA material, young's modulus of PLA and strain applied during tensile. Based on this equation, the porosity's geometric architecture does not contribute to the stress value, so changing the porosity did not affect the stress value.

Meanwhile, the magnitude of the maximum tensile load act on the bone scaffold disk was influenced by the cross-section area of the vertical columns, which they can hold. The magnitude of the applied force can be defined as stress distributed over the holding cross-section area. The smaller the porosity, the bigger the column, which increases the capability of the bone scaffolds. As the porosity increased, the column size reduced, and at the same time, the tensile force capture during the tensile test also reduced. Thus, matching the bone scaffold's pore size and capability is required in bone regeneration to ensure that the important aspect of the strength and the bone remodelling process can be fulfilled.

## 5. Conclusions

In conclusion, this study focused on the analysis structure's fracture based on the Finite Element Analysis (FEA) and comparing it with experimental data for bone scaffold samples with varying porosity levels. The validated FEA was then used to investigate the effect of porosity on stress distribution and strength of the bone scaffold structure. The study found that increasing porosity decreased the maximum tensile force the scaffold can support, with an average reduction of 64% and 55% for FEA and experimental data, respectively. The difference between FEA and experimental results can be attributed to structural differences between the models used in the study.

This study's novelty lies in the comprehensive investigation of the relationship between porosity and the strength of the bone scaffold structure. The point at which the bone scaffold's stress distribution shifts from elastic to plastic deformation was identified and the variation in maximum tensile force reduction with increasing porosity was discussed in detail. Additionally, the study highlights the importance of validating FEA with experimental data and the potential limitations of FEA due to structural differences between models and experimental samples. The information can be used to develop bone scaffold structures by improving their strength and resistance to fracture.

The main finding of the study can be concluded as follows:

- Maximum tensile stress that the structure can hold increases with decreasing of bone scaffold porosity, which lower porosity higher the maximum stress the structure can hold
- Under the tensile test, the vertical column holds most of the applied load, indicating higher stress than the horizontal column. Its cross-section area is important to determine the strength of the structure
- Even though porosity varied the maximum tensile force that the structure could hold, the magnitude of the stress across the bone scaffold is similar for all samples as the stress value is the function of the young's modulus of the material and applied strain.

**Acknowledgement**

This study was supported by Universiti Teknologi MARA, UiTM, under Grant Penyelidikan MyRA (file number 600-RMC/GPM LPHD 5/3 (110/2021)).

### Nomenclatures

| | |
|---|---|
| $D$ | Sample diameter |
| $d$ | Loading hole |
| $L$ | Sample width |
| $M$ | Notch length |
| $W$ | Distance |

***Greek Symbols***

| | |
|---|---|
| $\varepsilon_{true}$ | True strain |
| $\varepsilon_{eng}$ | Engineering strain |

| | |
|---|---|
| $\sigma_{true}$ | True stress |
| $\sigma_{eng}$ | Engineering strain |

**Abbreviations**

| | |
|---|---|
| ASTM | American Society for Testing and Materials |
| CFD | Computational fluid dynamic |
| FEA | Finite element analysis |
| PLA | Polylactic acid |

## References


1. Ghassemi, T.; Shahroodi, A.; Ebrahimzadeh, M.H.; Mousavian, A.; Movaffagh, J.; and Moradi, A. (2018). Current concepts in scaffolding for bone tissue engineering. *Archives of Bone and Joint Surgery*, 6(2), 90-99.
2. Mehboob, A.; Mehboob, H.; and Chang, S. H. (2020). Evaluation of unidirectional BGF/PLA and Mg/PLA biodegradable composites bone plates-scaffolds assembly for critical segmental fractures healing. *Composites Part A: Applied Science and Manufacturing*, 135, 105929.
3. Bahraminasab, M.; Janmohammadi, M.; Arab, S.; Talebi, A.; Nooshabadi, V.T.; Koohsarian, P.; and Nourbakhsh, M.S. (2021). Bone scaffolds: an incorporation of biomaterials, cells, and biofactors. *ACS Biomaterials Science & Engineering*, 7(12), 5397-5431.
4. Murphy, C.M.; and O'Brien, F.J. (2010). Understanding the effect of mean pore size on cell activity in collagen-glycosaminoglycan scaffolds. *Cell & Adhesion Migrations*, 4(3), 377-381.
5. Danilevicius, P.; Georgiadi, L.; Pateman, C.J.; Claeyssens, F.; Chatzinikolaidou, M.; and Farsari, M. (2015). The effect of porosity on cell ingrowth into accurately defined, laser-made, polylactide-based 3D scaffolds. *Applied Surface Science*, 336, 2-10.
6. Maghami, E.; Moore, J.P.; Josephson, T.O.; and Najafi, A.R. (2022). Damage analysis of human cortical bone under compressive and tensile loadings. *Computer Methods in Biomechanics and Biomedical Engineering*, 25(3), 342-357.
7. Kang, Y.; Scully, A.; Young, D.A.; Kim, S.; Tsao, H.; Sen, M.; and Yang, Y. (2011). Enhanced mechanical performance and biological evaluation of a PLGA coated β-TCP composite scaffold for load-bearing applications. *European Polymer Journal*, 47(8), 1569-1577.
8. Byrne, D.P.; Lacroix, D.; Planell, J.A.; Kelly, D.J.; and Prendergast, P.J. (2007). Simulation of tissue differentiation in a scaffold as a function of porosity, Young's modulus and dissolution rate: application of mechanobiological models in tissue engineering. *Biomaterials*, 28(36), 5544-5554.
9. Lacroix, D.; Chateau, A.; Ginebra, M.P.; and Planell, J.A. (2006). Micro-finite element models of bone tissue-engineering scaffolds. *Biomaterials*, 27(30), 5326-5334.
10. Liu, Z.; Liang , H.; Shi, T.; Xie, D.; Chen R.; Han, X.; Shen, L.; Wang, C.; and Tian, Z. (2019). Additive manufacturing of hydroxyapatite bone scaffolds via digital light processing and in vitro compatibility. *Ceramics International*, 45(8), 11079-11086.

11. Carlsson, J.; Braesch-Andersen, A.; Ferguson, S.J.; and Isaksson, P. (2023). Fracture in porous bone analysed with a numerical phase-field dynamical model. *Journal of the Mechanical Behavior of Biomedical Materials*, 139, 105659.
12. Meena, T.; and Roy, S. (2022). Bone fracture detection using deep supervised learning from radiological images: A paradigm shift. *Diagnostics*, 12(10), 2420.
13. Pires, T.; Dunlop, J.W.; Fernandes, P.R.; and Castro, A.P. (2022). Challenges in computational fluid dynamics applications for bone tissue engineering. *Proceedings of the Royal Society A*, 478(2257), 20210607.
14. Milan, J.L.; Sandino, C.; Midderhoff, S.; Marques, L.; Planell, J.A.; and Lacroix, D.. (2009). Mode of failure of a biomaterial composite scaffold for bone tissue engineering using synchrotron micro-tomography and finite element analysis. *Proceedings of the 12th International Conference on Fracture (ICF)*, Ottawa, Canada, 1-8.
15. Yang, J.; Lian, H.; Liang, W.; Nguyen, V.P.; and Bordas, S.P.A. (2019). Model I cohesive zone models of different rank coals. *International Journal of Rock Mechanics and Mining Sciences*, 115, 145-156.
16. Lemesle, J.; Hubert, C.; and Bigerelle, M. (2020). Numerical study of the toughness of complex metal matrix composite topologies. *Applied Sciences*, 10(18), 6250.
17. Khosravani, M.R.; Berto, F.; Ayatollahi, M. R.; and Reinicke, T. (2020). Fracture behavior of additively manufactured components: A review. *Theoretical and Applied Fracture Mechanics*, 109, 102763.
18. Huo, P.; Zhao, Z.; Bai, P.; Yuan, X.; Wang, Q.; Zhao, R.; Zhang, L.; Du, W.; Han, B.; and Wang, Y. (2021). Deformation evolution and fracture mechanism of porous TC4 alloy scaffolds fabricated using selective laser melting under uniaxial compression. *Journal of Alloys and Compounds*, 861, 158529.
19. Mohammadi-Zerankeshi, M.; and Alizadeh, R. (2023). 3D-printed PLA-Gr-Mg composite scaffolds for bone tissue engineering applications. *Journal of Materials Research and Technology*, 22, 2440-2446.
20. Deng, F.; Liu, L.; Li, Z.; and Liu, J. (2021). 3D printed Ti6Al4V bone scaffolds with different pore structure effects on bone ingrowth. *Journal of Biological Engineering*, 15(1), 4.
21. Yang, Y.; Wang, G.; Liang, H.; Peng, S.; Shen, L.; and Shuai, C. (2019). Additive manufacturing of bone scaffolds. *International Journal of Bioprinting*, 5(1), 148.
22. Jia, Z.; and Wang, L. (2019). 3D printing of biomimetic composites with improved fracture toughness. *Acta Materialia*, 173, 61-73.
23. Wang, X.; Zhao, L.; Fuh, J.Y.H.; and Lee, H.P. (2019). Effect of porosity on mechanical properties of 3D printed polymers: Experiments and micromechanical modeling based on X-ray computed tomography analysis. *Polymers*, 11(7), 1154.
24. Pernica, J.; Sustr, M.; Dostal, P.; Brabec, M.; and Dobrocky, D. (2021). Tensile testing of 3D printed materials made by different temperature. *Manufacturing Technology*, 21(3), 398-404.
25. Banjanin, B.; Vladić, G.; Pál, M.; Baloš, S.; Dramićanin, M.; Rackov, M.; and Kneţević, I. (2018). Consistency analysis of mechanical properties of elements produced by FDM additive manufacturing technology. *Revista Matéria*, 23(4), 1-15.

26. Wang, Z., Huang, C.; Wang, J.; Wang, P.; Bi, S.; and Abbas, C.A. (2019). Design and simulation of flow field for bone tissue engineering scaffold based on triply periodic minimal surface. *Chinese Journal of Mechanical Engineering*, 32(1), 1-10.
27. Srinivasan, M.; and Seetharamu, S. (2012). Fracture toughness of metal castings. *Science and Technology of Casting Processes*, 285-312.
28. ASTM E. (1820). Standard test method for measurement of fracture toughness. *ASTM, Annual Book of Standards*, 3.
29. Baheti, V.; Militky, J.; and Ul Hassan, S. Z. (2013). Polylactic Acid (PLA) Composite Films Reinforced with Wet Milled Jute Nanofibers. *Paper presented at the Conference Papers in Materials Science*,
30. Aliheidari, N.; Tripuraneni, R.; Ameli, A.; and Nadimpalli, S. (2017). Fracture resistance measurement of fused deposition modeling 3D printed polymers. *Polymer Testing*, 60, 94-101.
31. Hannink, G.; and Arts, J. C. . (2011). Bioresorbability, porosity and mechanical strength of bone substitutes: What is optimal for bone regeneration? *Injury*, 42, S22-S25.